Nanoscale Contact Line Pinning Boosted by Ångström-Scale Surface Heterogeneity

Heima, Yuta
Department of Aeronautics and Astronautics, Kyushu University

Teshima, Hideaki
Department of Aeronautics and Astronautics, Kyushu University

Takahashi, Koji
Department of Aeronautics and Astronautics, Kyushu University

出版情報：The Journal of Physical Chemistry Letters. 14 (14), pp.3561-3566, 2023-04-05. American Chemical Society
バージョン：

Nanoscale Contact Line Pinning Boosted by Ångström-Scale Surface Heterogeneity

Yuta Heima [a], *Hideaki Teshima** [a, b], *Koji Takahashi* [a, b]

[a] Department of Aeronautics and Astronautics, Kyushu University, Nishi-Ku, Motooka 744, Fukuoka 819-0395, Japan

[b] International Institute for Carbon-Neutral Energy Research (WPI-I2CNER), Kyushu University, Nishi-Ku, Motooka 744, Fukuoka 819-0395, Japan

*E-mail: hteshima05@aero.kyushu-u.ac.jp

ABSTRACT

The pinning effect plays an important role in many fluidic systems but remains poorly understood, especially at the nanoscale. In this study, we measured the contact angles of glycerol nanodroplets on three different substrates using atomic force microscopy. By comparing the shapes of the three-dimensional images of droplets, we found that a possible origin of the long-discussed deviation of the contact angles of nanodroplets from the macroscopic value is the pinning force induced by ångström-scale surface heterogeneity. It was also revealed that the pinning forces acting on glycerol nanodroplets on a silicon dioxide surface are up to twice as large as those acting on macroscale droplets. On a substrate where the effect of pinning was strong, an unexpected irreversible change from an irregularly shaped droplet to an atomically flat liquid film occurred. This was explained by the transition of the dominant force from liquid/gas interfacial tension to an adsorption force.

TOC GRAPHICS

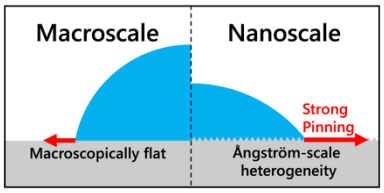

KEYWORDS

Pinning, Contact angle, Nanodroplets, Surface heterogeneity

As the system size decreases, the forces governing physical phenomena shift from volume forces to surface forces, dramatically changing important fluid parameters, such as flow velocity[1], vapor pressure[2,3], intermolecular structure[4], ion transport[5], dielectric constant[6], refractive index[7], and viscosity[8]. The increased surface-interaction effects on molecules and ions cause the fluid to behave differently at small scales than in bulk systems[9,10]. For example, superstable water films form in open-ended carbon nanotubes under high-vacuum conditions ($<10^{-5}$ pa)[2,3] and ultrafast water permeation occurs through fluorous nanochannels[11]. In particular, wetting phenomena at the nanoscale have attracted significant interest owing to their importance in the development of nanofluidic devices that take advantage of unique fluid behavior for the separation and analysis of chemical species and biomolecules[12,13], for desalination[11], and for cooling in electronic devices[14,15].

To date, much scientific effort has been devoted to understanding nanoscale wetting phenomena. However, we still do not know how small droplets wet the surface, and there are discrepancies between experimental and simulation results. Specifically, it has been reported based on molecular dynamics (MD) analysis that on ideal solid surfaces, Young's equation, which describes equilibrium contact angles as the relationships among solid/liquid, solid/gas, and liquid/gas interfacial tensions, holds for nanoscopic droplets[16] and bubbles[17], just as it does for macroscopic systems. By contrast, atomic force microscopy (AFM) studies have reported that the contact angles of nanodroplets and nanobubbles on real solid surfaces depend on their size[18–20], which cannot be explained by classical Young's equation. Models have been proposed to explain this dependence of the contact angle on size by taking into consideration the effects of line tension[21], disjoining pressure[22], and nanoscale distribution of hydrophilic and hydrophobic regions[23]; however, the main determining factors have not yet been elucidated. This size dependence of the contact angle

prevents the evaluation of nanoscale wettability based on the contact angle, making it difficult to predict fluid behavior caused by wetting.

Pinning is also an important determinant of fluid behavior. Pinning is caused by the structural and chemical heterogeneity of solid surface[24,25] and can result in the contact angle varying from the equilibrium contact angle, which is termed contact angle hysteresis. In contrast with nanodroplets, some of the unique features of surface nanobubbles, such as their extremely flat shape and superstability toward disturbance, have been explained by pinning[26–28]. However, despite the importance of pinning in interfacial phenomena, it is still unclear how it works at the nanoscale. In the present work, we measured nanodroplets nucleated on substrates with different surface properties using AFM. We discovered for the first time that surface heterogeneity on the order of the ångström boosts the nanoscale pinning force, which causes the deviation from the macroscopic contact angle and the transformation of the fluid from an irregular shape to an atomically flat liquid film.

A silicon (Si) substrate, Si substrate with a 300-nm-thick silicon dioxide (SiO_2) film formed by thermal oxidation and highly oriented pyrolytic graphite (HOPG) were used as substrates for nanodroplet observations. The Si and SiO_2 substrates were cleaned by ultrasonication in acetone for 20 minutes before use. The topmost layer of the HOPG was peeled off with Scotch tape (3M) to expose a clean surface. The average roughness (Ra) of each substrate was measured using AFM in areas without step structure and impurities. The Ra values and their standard deviations were 0.268 ± 0.040, 0.222 ± 0.033, and 0.066 ± 0.016 nm for Si, SiO_2, and HOPG, respectively. The surface-height images and cross-sectional profiles of each substrate measured by AFM are shown in Fig. 1. The number of peaks with a height greater than 0.1 nm in the cross-sectional profile was 33 for Si, 16 for SiO_2, and 2 for HOPG. Because HOPG is composed of stacked graphene, its

surface is extremely flat. The SiO_2 surface was rougher than the HOPG surface, with ångström-order roughness. Si had a similar surface topography to SiO_2, but was rougher than SiO_2, as confirmed by the Ra and cross-sectional profiles. The macroscopic equilibrium contact angles of glycerol droplets were 76.7° on Si, 71.4° on SiO_2, and 40.1° on HOPG (see Supplementary material).

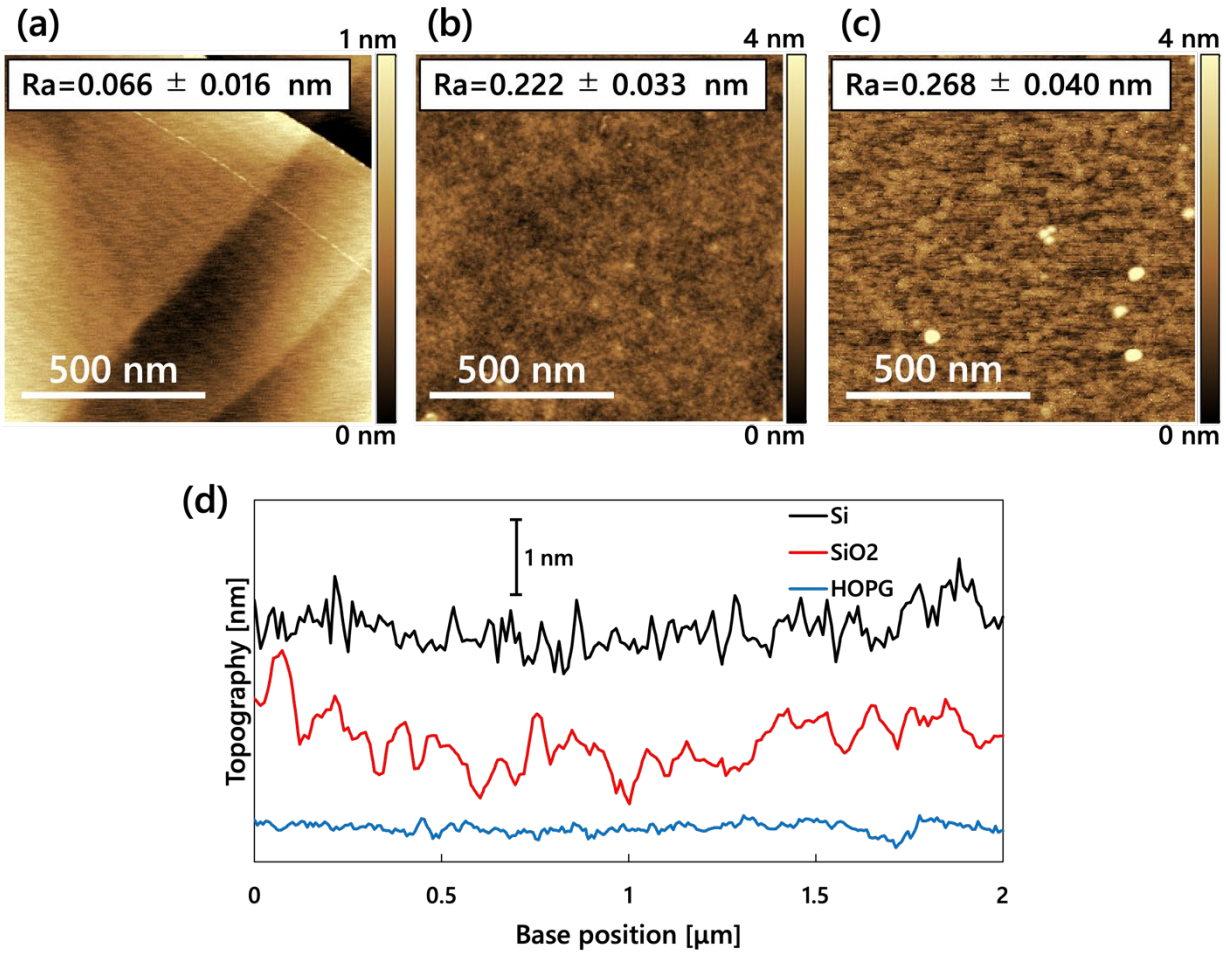

Fig. 1 Height images of (a) HOPG, (b) SiO_2, and (c) Si surfaces (1 μm × 1 μm), and (d) their cross-sectional profiles measured by AFM.

Glycerol was used for nanodroplet nucleation according to some requirements for the measurements. Specifically, the liquid to be used for AFM measurements must have a low vapor pressure to remain stable during the measurement. Additionally, it must have a high liquid-gas interfacial tension. If the interfacial tension is low, the liquid wets the probe, interrupting the measurement and making it difficult to successfully measure the shape of nanodroplets. Glycerol nanodroplets were generated on each substrate using a previously reported method[21]. First, a drop of glycerol with a diameter of approximately 10 mm was placed on a glass slide, which was then placed on a heating stage set at 160 °C. The heated glycerol droplet generated a mist and vapor. The substrates were held approximately 10 mm above the heated droplet for several seconds. This process produces micro- and nanodroplets on the substrate surface facing the heater by adhesion of the mist and/or by condensation of the vapor. We note that the mist was visible to the naked eye, indicating that the size of the droplets was larger than approximately 1 μm. There were many microdroplets on the substrate surface (see the Supplementary material). However, the diameter of the nanodroplets observed using AFM, which is discussed later, was less than 1 μm, suggesting that they were generated by the direct adhesion of smaller nanodroplets or by vapor condensation.

The amplitude-modulation (AM) mode of AFM (SPM-8100FM, Shimadzu Corp., Japan) and OPUS 200AC-NA cantilevers (MikroMasch, Bulgaria; tip radius, <7 nm; resonant frequency, 85–175 kHz; spring constant, 3–22 N/m) were used to characterize the three-dimensional profiles of the substrate surfaces and the nanodroplets. The measurements were performed in a thermostatic chamber at room temperature to minimize the influence of the ambient environment. In addition, to avoid the effect of water-vapor condensation[29], the humidity inside the chamber was kept below 20% during the experiments.

The images obtained from AFM measurements of the substrates on which nanodroplets were generated are shown in Fig. 2. Droplets with base diameters of approximately 20–700 nm were observed on the SiO_2 and HOPG surfaces. Specifically, on the HOPG [Fig. 2(a), Fig. S3 in Supplementary material], the nanodroplets were distributed in a line along steps on the surface. This is because the step edges are more hydrophilic than the surrounding defect-free terrace regions[30]. This row-like formation of the droplets has also been reported in condensation experiments[30,31], suggesting that the nanodroplets observed in our AFM experiment were mostly formed by the condensation of glycerol molecules, not by the direct depositions of the droplets. On SiO_2 [Fig. 2(b)], spherical nanodroplets were randomly generated. By contrast, no spherical nanodroplets were observed on Si, and irregularly shaped droplets with highly distorted contact lines were formed (discussed later).

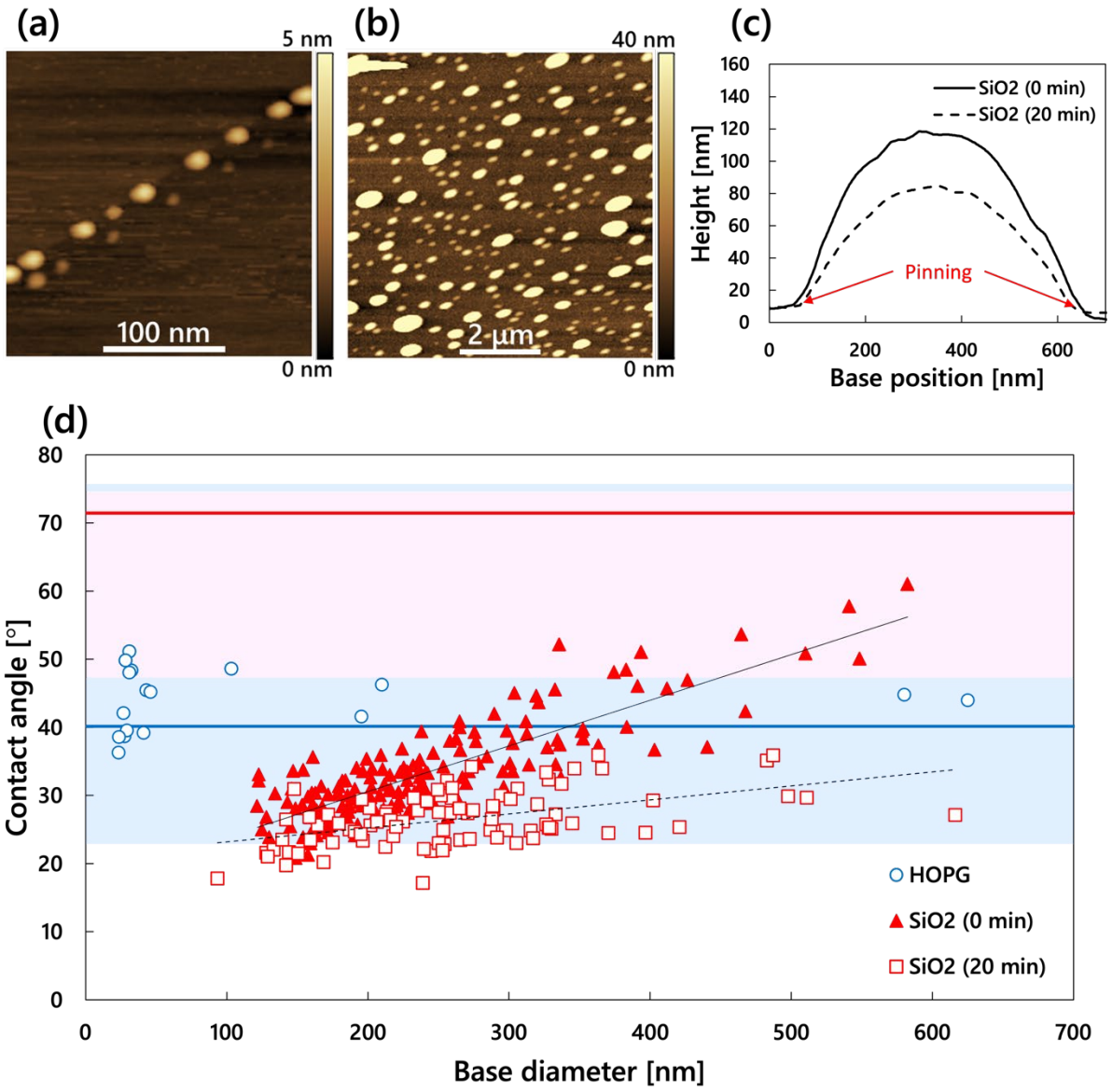

Fig. 2. AFM height images of glycerol nanodroplets on (a) HOPG (250 nm × 250 nm) and (b) SiO_2 (7.5 μm × 7.5 μm) surfaces. (c) Cross-sectional profiles of a nanodroplet on SiO_2 at 0 and 20 minutes. (d) Relationship between the base diameter and contact angle of nanodroplets on HOPG and SiO_2. The blue and red solid lines represent the contact angles of the macroscopic droplets on HOPG and SiO_2, respectively. The light blue and pink regions represent the macroscopic contact angle hysteresis of HOPG and SiO_2, respectively. The black solid and dashed lines are linear-

approximate straight lines obtained by least-squares fitting of the scatter at 0 minutes (Fig. 2(a)) and 20 minutes (see Fig. S4(b) in Supplementary material) on SiO_2, respectively.

The relationship between the contact angle and base diameter is shown in Fig. 2(d). The contact angles were calculated from the cross-sections of the nanodroplets. The nanodroplets on the HOPG surface showed a contact angle of approximately 40° regardless of their size, which was almost the same as that of the macroscopic droplets (40.1°). This suggests that the contact angles of the nanodroplets on the HOPG surface are determined by the balance of the interfacial tensions as they are in macroscopic systems (that is, as described by Young's equation). By contrast, the contact angles of nanodroplets on SiO_2, which were widely distributed in the range of 13°–61°, were smaller than that of the macroscopic droplets (71.4°). In addition, the plot shows a clear dependence of the contact angle on the base diameter, which is consistent with the results reported in previous studies[21–23,29,32]. However, when the same area was measured 20 minutes later (indicated by the square symbols), the dependence became weaker, which means that the droplets shrunk only in height. We note that the volume reduction may be due to the accelerated evaporation caused by the laser irradiation of the AFM probe. Thus, at the nanoscale, Young's equation holds for the HOPG surface but not for the SiO_2 surface.

Models have been proposed to explain the dependence of the contact angle on the droplet size at the nanoscale. For example, Checco et al.[23] proposed that it is due to the wettability distributions on the solid surface. They assumed that there are nanoscale distributions of relatively high and low wettability on the surface and that droplets start to nucleate at the most hydrophilic positions to minimize the surface free energy. As the droplet grows, the proportion of hydrophobic regions in the contact area increases, resulting in a larger contact angle for larger droplets. However, in the

present study, as shown in Fig. 2(c) and (d), many droplets were observed the contact angles of which decreased without changing the base area after shrinking. Thus, the local wettability of the contact surface cannot explain the size dependence of the droplet contact angle. Ma et al.[22] explained the dependence by introducing a disjoining pressure. Specifically, by calculating the disjoining pressure due to the van der Waals force acting on the gas/liquid interface of the droplet, they proposed that the force to deform the droplet due to the disjoining pressure is balanced with the force to return the deformation of the droplet due to the imbalance of the interfacial tension at the three-phase contact line. In the present study, however, the droplet deformation was much larger than that in their study, and the force induced by the disjoining pressure was calculated to be approximately 1/40 of that required to deform the droplet (see the Supplementary material). Therefore, the size dependence of the contact angle cannot be explained by the effect of van der Waals force-induced disjoining pressure. Heim and Bonaccurso[21] re-defined the line tension as a variable of the contact angle to explain the contact angle dependence of ionic liquid nanodroplets. However, in the present study, the size dependence of the contact angle on SiO_2 surfaces weakened after 20 minutes (Fig. 2(d)), indicating that the line tension does not depend on the contact angle. Therefore, this dependence cannot be explained by the line tension. From these observations, we conclude that it is difficult to explain the dependence of the contact angle on the droplet size using existing models.

We propose that the contact angle dependence on the base diameter is due to the pinning effect, which allows droplets to have a wide range of contact angles by fixing the contact line. The cross-sections of the same droplet [Fig. 2(c)] show that the height decreased while the base diameter remained almost constant. This behavior is known as a constant contact radius mode in the context of droplet condensation and is observed during the evaporation of "pinned" macroscopic droplets[33],

strongly suggesting that the contact line was pinned. The relationship between the contact angle distribution and the base diameter shown in Fig. 2(d) has also been reported for pinned nanobubbles[20].

The pinning force acts on the three-phase contact line in balance with interfacial tensions. Considering the pinning force, Young's equation can be modified as follows[20].

$$\cos\theta = \cos\theta_{\mathrm{macro}} - \frac{F_{\mathrm{p}}}{\gamma_{\mathrm{LG}}} \tag{1}$$

where γ_{LG} is the liquid/gas interfacial tension, F_{p} is the pinning force, θ_{macro} is the contact angle of the macroscopic droplet, and θ is the droplet contact angle. Here, γ_{LG} is 63.4 mN/m[34] for glycerol. The advancing and receding contact angles of the macroscopic droplet on the SiO_2 surface were $\theta_{\mathrm{adv}} = 75°$ and $\theta_{\mathrm{rec}} = 49°$, respectively (see the Supplementary materials). Thus, according to eq. (1) and $\theta_{\mathrm{macro}} = 71.4°$, the range of the pinning force is −4 to 21 mN/m for macroscopic droplets. However, surprisingly, the pinning force acting on the nanodroplets is 10–41 mN/m, indicating that, for a glycerol droplet on SiO_2, it becomes approximately twice as strong as that working on the macroscale droplets. It should be noted that the doubling of the maximum pinning force is specific to the combination of glycerol and SiO_2, and may vary depending on the liquid and solid surface. Moreover, the step structures and impurities displayed on HOPG and Si surfaces will not be the cause of the nanoscale pinning effect (refer to the Supplementary materials). Also, further analysis of the pinning force acting on all nanodroplets is shown in Fig. S9 in the Supplementary materials.

In contrast with the SiO_2 surface, the contact angles of the nanodroplets on the HOPG surface were almost in the range of the macroscopic contact angle hysteresis (Fig. 2(d)). This is because of the difference in surface topography. As mentioned above, HOPG is ideally smooth, whereas the SiO_2 and Si surfaces have ångström-order roughness (Fig. 1). We propose that the small surface

heterogeneity only influences the nanoscale droplets because the ratio of the liquid/gas interface deformed by the solid surface to the total liquid/gas interface increases as the droplets become smaller, and the distortion of the three-phase contact line becomes larger relative to the size of the droplet. That is to say, by decreasing the droplet size, the ångström-order roughness changes from weak heterogeneity that is negligible for contact angle hysteresis to strong heterogeneity[35], resulting in enhanced nanoscale pinning. Indeed, a stronger pinning force acted on the smaller droplets, as shown in Fig. 2(d). This is consistent with MD simulation results showing that the pinning effects due to small roughness become negligible when the droplet size increases[36]. Similarly, it has also been demonstrated in condensation phenomena that nanoscale roughness affects wetting.[37]

We also found that a strong pinning force induces an unexpected transformation of the nanoscale fluid, which is important knowledge for the development of nanofluidics. Specifically, on the Si surface, in contrast to the HOPG and SiO_2 surfaces, spherical droplets were not observed but irregularly shaped thin droplets with a thickness of several nanometers appeared, as shown in Fig. 3. Their three-phase contact line was highly distorted, and the local contact angles varied in the range of 3°–14°, indicating strong pinning at the contact line. Because such strong distortion was not observed on the SiO_2 surface, we suggest that the Si surface provides the strongest pinning force among the substrates used in our experiments. This result may be attributed to the fact that the surface roughness of Si (Ra = 0.268 nm) is the largest among the three substrates, resulting in a strong pinning force induced by the geometrical heterogeneity. Moreover, the Si surface is known to have a natural oxide layer containing impurities during its formation[38,39], which may cause chemical heterogeneity in addition to geometrical heterogeneity.

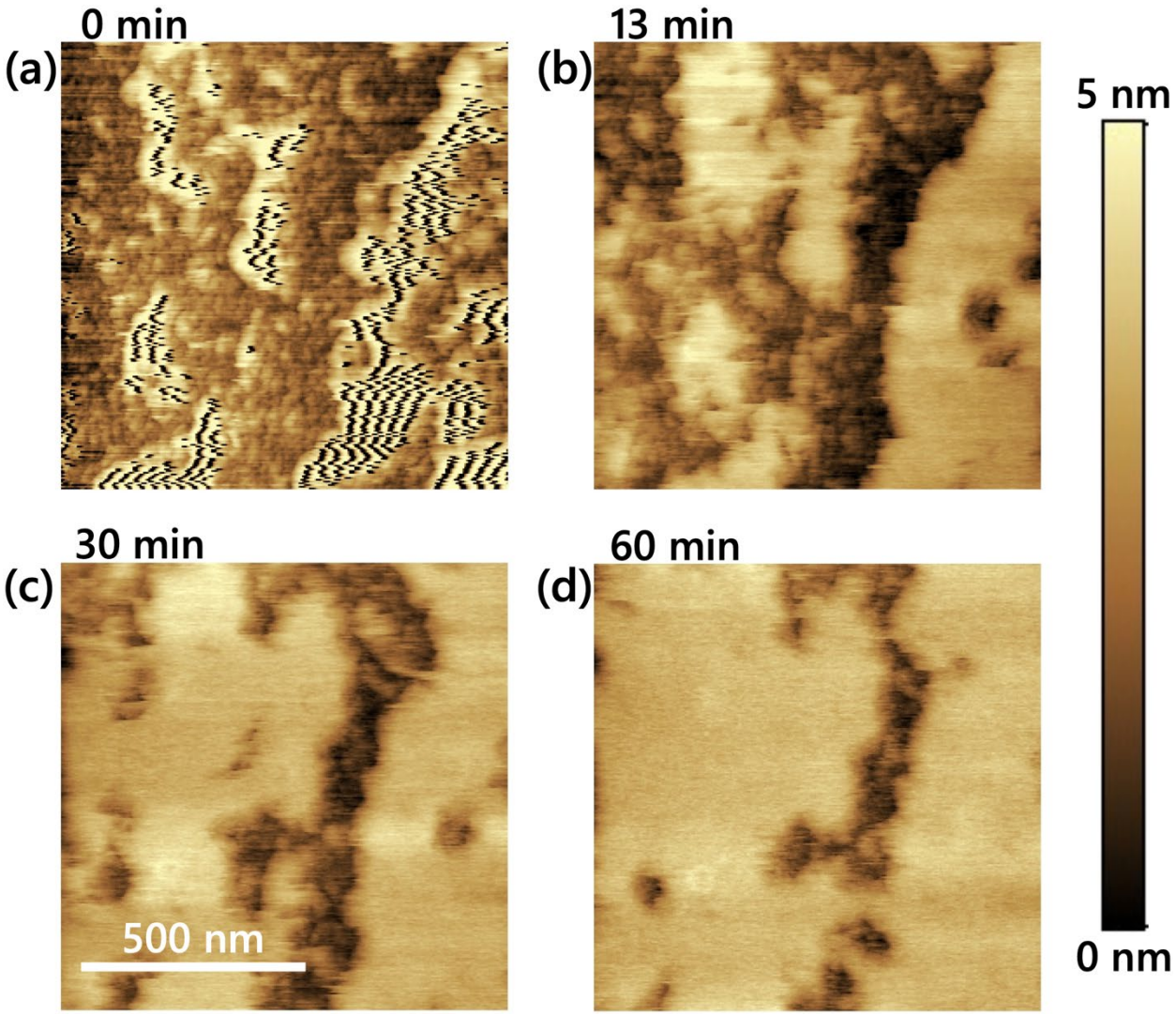

Fig. 3 AFM height images of liquid films on Si substrates and their shape evolution during repeated measurements. The images were taken at (a) 0 minutes, (b) 13 minutes, (c) 30 minutes, and (d) 60 minutes after the completion of the first image. We note that the zigzag-shaped texture in (a) is a scanning error induced by the penetration of the AFM probe and does not reflect the actual height.

In Fig. 3(a), a zigzag texture can be seen in the irregularly shaped droplet, which was sometimes also observed on the droplets (see Supplementary material). This is a scan error caused by the formation of a meniscus on the AFM tip, which interferes with the scanning because of the

liquid/gas interfacial tension. This paradoxically proves that there is a droplet thick enough for the liquid/gas interfacial tension to act. As shown in Fig. 3(b–d), the droplet laterally expanded during repeated measurements at the same position. This may be due to the contact of the AFM probe during measurement, which presses down and expands the droplet, resulting in a thinner and wider droplet. Eventually, the thickness of the film was almost constant over the entire region at 2.5–3.0 nm, which corresponds to four or five layers of glycerol with a molecular diameter of approximately 0.6 nm[40]. In addition, as the film expanded, the zigzag-shaped texture disappeared. This transformation was only observed on the Si surface and not on the HOPG or SiO_2 surfaces. Moreover, once the film became thin, it did not return to its initial thickness, implying that the transformation was irreversible.

The mechanism of the irreversible transformation is explained as follows. First, the flattened shape induced by AFM scanning is maintained by the strong pinning force of the Si surface. As the film becomes thin, the liquid/gas interfacial tension weakens because the bulk density region disappears[17] and the attractive surface force between the liquid molecules and the substrate (i.e., the adsorption force) becomes dominant. Finally, the molecular-scale-thickness layer becomes flat over the entire region and behaves like a solid because of the strong adsorption force on the solid surface. Such an adsorption-induced phase change has also been reported for gas molecules adsorbed at a solid/liquid interface[41]. We note that the smallest contact angle of the nanodroplets observed on SiO_2 was approximately 13°, which should correspond to the maximum pinning force on the surface. Therefore, even if the droplet is temporarily flattened below the smallest contact angle by the scanning, the shape cannot be retained by the pinning. This is why a flat film like that on the Si substrate was not observed on the SiO_2 surface.

In summary, using AM-AFM, we measured the morphology of glycerol nanodroplets generated on substrates with different surface heterogeneity to investigate the nanoscale pinning effect. Our results indicate that the nanoscale pinning effect is boosted by ångström-scale surface heterogeneity, which is up to twice as strong as that for macrodroplets. This pinning effect is a promising candidate mechanism to explain the origin of long-discussed size dependence of the contact angle of nanodroplets. Furthermore, it was found that the strongest pinning effect due to the geometrical and chemical heterogeneity of the Si surface can induce a novel transformation of a thick and irregular shape to an atomically flat liquid film. Our results demonstrate the importance of fine surface roughness in nanofluidics, which has previously been assumed to be negligible, and extend our knowledge of the dynamics of the three-phase contact line.

ASSOCIATED CONTENT

The Supporting Information is available free of charge at xxxxx

Includes contact angle images on each substrate, optical microscope image of microdroplets, AFM image of large droplets on the HOPG surface, AFM images before and after volume change of droplets on SiO_2 and HOPG, cross-sectional profiles of a nanodroplet on HOPG, calculation of disjoining pressure caused by van der Waals force, consideration of the effect of step structures and spherical impurities on the pinning effect, graph of the relationship between the base diameter and pinning force working on nanodroplets and a zigzag texture observed on the nanodroplet.

AUTHOR INFORMATION

Corresponding Author

Hideaki Teshima

*E-mail: hteshima05@aero.kyushu-u.ac.jp

ORCID

Hideaki Teshima: 0000-0002-9240-3370

Koji Takahashi: 0000-0002-3552-9292

Notes

The authors declare no competing financial interest.

ACKNOWLEDGMENT

This work was supported by JST CREST Grant No. JPMJCR18I1, JST SPRING, Grant No. JPMJSP2136, and JSPS KAKENHI Grant No. JP20H02089, JP21K20405, JP22K14193, JP22K18772. We thank Yuki Ishihara for his support of AFM measurements.

REFERENCES

(1) Nair, R. R.; Wu, H. A.; Jayaram, P. N.; Grigorieva, I. V.; Geim, A. K. Unimpeded Permeation of Water through Helium-Leak-Tight Graphene-Based Membranes. *Science* **2012**, *335* (6067), 442–444.

(2) Tomo, Y.; Askounis, A.; Ikuta, T.; Takata, Y.; Sefiane, K.; Takahashi, K. Superstable Ultrathin Water Film Confined in a Hydrophilized Carbon Nanotube. *Nano Lett.* **2018**, *18* (3), 1869–1874.

(3) Li, Q.-Y.; Matsushita, R.; Tomo, Y.; Ikuta, T.; Takahashi, K. Water Confined in Hydrophobic Cup-Stacked Carbon Nanotubes beyond Surface-Tension Dominance. *J. Phys. Chem. Lett.* **2019**, *10* (13), 3744–3749.

(4) Algara-Siller, G.; Lehtinen, O.; Wang, F. C.; Nair, R. R.; Kaiser, U.; Wu, H. A.; Geim, A. K.; Grigorieva, I. V. Square Ice in Graphene Nanocapillaries. *Nature* **2015**, *519* (7544), 443–445.

(5) Gopinadhan, K.; Hu, S.; Esfandiar, A.; Lozada-Hidalgo, M.; Wang, F. C.; Yang, Q.; Tyurnina, A. V.; Keerthi, A.; Radha, B.; Geim, A. K. Complete Steric Exclusion of Ions and Proton Transport through Confined Monolayer Water. *Science* **2019**, *363* (6423), 145–148.

(6) Fumagalli, L.; Esfandiar, A.; Fabregas, R.; Hu, S.; Ares, P.; Janardanan, A.; Yang, Q.; Radha, B.; Taniguchi, T.; Watanabe, K.; Gomila, G.; Novoselov, K. S.; Geim, A. K. Anomalously Low Dielectric Constant of Confined Water. *Science* **2018**, *360* (6395), 1339–1342.

(7) Le, T. H. H.; Morita, A.; Tanaka, T. Refractive Index of Nanoconfined Water Reveals Its Anomalous Physical Properties. *Nanoscale Horiz* **2020**, *5* (6), 1016–1024.

(8) Neek-Amal, M.; Peeters, F. M.; Grigorieva, I. V.; Geim, A. K. Commensurability Effects in Viscosity of Nanoconfined Water. *ACS Nano* **2016**, *10* (3), 3685–3692.

(9) Kavokine, N.; Netz, R. R.; Bocquet, L. Fluids at the Nanoscale: From Continuum to Subcontinuum Transport. *Annu. Rev. Fluid Mech.* **2021**, *53* (1), 377–410.

(10) Zhang, X.; Liu, H.; Jiang, L. Wettability and Applications of Nanochannels. *Adv. Mater.* **2019**, *31* (5), e1804508.

(11) Itoh, Y.; Chen, S.; Hirahara, R.; Konda, T.; Aoki, T.; Ueda, T.; Shimada, I.; Cannon, J. J.; Shao, C.; Shiomi, J.; Tabata, K. V.; Noji, H.; Sato, K.; Aida, T. Ultrafast Water Permeation through Nanochannels with a Densely Fluorous Interior Surface. *Science* **2022**, *376* (6594), 738–743.

(12) Abgrall, P.; Nguyen, N. T. Nanofluidic Devices and Their Applications. *Anal. Chem.* **2008**, *80* (7), 2326–2341.

(13) Tegenfeldt, J. O.; Prinz, C.; Cao, H.; Huang, R. L.; Austin, R. H.; Chou, S. Y.; Cox, E. C.; Sturm, J. C. Micro- and Nanofluidics for DNA Analysis. *Anal. Bioanal. Chem.* **2004**, *378* (7), 1678–1692.

(14) van Erp, R.; Soleimanzadeh, R.; Nela, L.; Kampitsis, G.; Matioli, E. Co-Designing Electronics with Microfluidics for More Sustainable Cooling. *Nature* **2020**, *585* (7824), 211–216.

(15) Wang, M.; Sun, H.; Cheng, L. Enhanced Heat Transfer Characteristics of Nano Heat Exchanger with Periodic Fins: A Molecular Dynamics Study. *J. Mol. Liq.* **2021**, *341*, 116908.

(16) Yamaguchi, Y.; Kusudo, H.; Surblys, D.; Omori, T.; Kikugawa, G. Interpretation of Young's Equation for a Liquid Droplet on a Flat and Smooth Solid Surface: Mechanical and Thermodynamic Routes with a Simple Lennard-Jones Liquid. *J. Chem. Phys.* **2019**, *150* (4), 044701.

(17) Teshima, H.; Kusudo, H.; Bistafa, C.; Yamaguchi, Y. Quantifying Interfacial Tensions of Surface Nanobubbles: How Far Can Young's Equation Explain? *Nanoscale* **2022**, *14* (6), 2446–2455.

(18) Xu, C.; Peng, S.; Qiao, G. G.; Gutowski, V.; Lohse, D.; Zhang, X. Nanobubble Formation on a Warmer Substrate. *Soft Matter* **2014**, *10* (39), 7857–7864.

(19) Wang, X.; Zhao, B.; Ma, W.; Wang, Y.; Gao, X.; Tai, R.; Zhou, X.; Zhang, L. Interfacial Nanobubbles on Atomically Flat Substrates with Different Hydrophobicities. *Chemphyschem* **2015**, *16* (5), 1003–1007.

(20) Teshima, H.; Nishiyama, T.; Takahashi, K. Nanoscale Pinning Effect Evaluated from Deformed Nanobubbles. *J. Chem. Phys.* **2017**, *146* (1), 014708.

(21) Heim, L.-O.; Bonaccurso, E. Measurement of Line Tension on Droplets in the Submicrometer Range. *Langmuir* **2013**, *29* (46), 14147–14153.

(22) Ma, J.; Jing, G.; Chen, S.; Yu, D. Contact Angle of Glycerol Nanodroplets under van Der Waals Force. *J. Phys. Chem. C Nanomater. Interfaces* **2009**, *113* (36), 16169–16173.

(23) Checco, A.; Guenoun, P.; Daillant, J. Nonlinear Dependence of the Contact Angle of Nanodroplets on Contact Line Curvature. *Phys. Rev. Lett.* **2003**, *91* (18), 186101.

(24) Paxson, A. T.; Varanasi, K. K. Self-Similarity of Contact Line Depinning from Textured Surfaces. *Nat. Commun.* **2013**, *4*, 1492.

(25) Encarnación Escobar, J. M.; García-González, D.; Dević, I.; Zhang, X.; Lohse, D. Morphology of Evaporating Sessile Microdroplets on Lyophilic Elliptical Patches. *Langmuir* **2019**, *35* (6), 2099–2105.

(26) Liu, Y.; Bernardi, S.; Widmer-Cooper, A. Stability of Pinned Surface Nanobubbles against Expansion: Insights from Theory and Simulation. *J. Chem. Phys.* **2020**, *153* (2), 024704.

(27) Lohse, D.; Zhang, X. Pinning and Gas Oversaturation Imply Stable Single Surface Nanobubbles. *Phys. Rev. E Stat. Nonlin. Soft Matter Phys.* **2015**, *91* (3), 031003.

(28) Dockar, D.; Borg, M. K.; Reese, J. M. Mechanical Stability of Surface Nanobubbles. *Langmuir* **2019**, *35* (29), 9325–9333.

(29) Xu, L.; Salmeron, M. Scanning Polarization Force Microscopy Study of the Condensation and Wetting Properties of Glycerol on Mica. *J. Phys. Chem. B* **1998**, *102* (37), 7210–7215.

(30) Zach, M. P.; Newberg, J. T.; Sierra, L.; Hemminger, J. C.; Penner, R. M. Chemical Vapor Deposition of Silica Micro- and Nanoribbons Using Step-Edge Localized Water. *J. Phys. Chem. B* **2003**, *107* (23), 5393–5397.

(31) Yamada, Y.; Ikuta, T.; Nishiyama, T.; Takahashi, K.; Takata, Y. Droplet Nucleation on a Well-Defined Hydrophilic-Hydrophobic Surface of 10 Nm Order Resolution. *Langmuir* **2014**, *30* (48), 14532–14537.

(32) Moldovan, A.; Bota, P.-M.; Poteca, T. D.; Boerasu, I.; Bojin, D.; Buzatu, D.; Enachescu, M. Scanning Polarization Force Microscopy Investigation of Contact Angle and Disjoining Pressure of Glycerol and Sulfuric Acid on Highly Oriented Pyrolytic Graphite and Aluminum. *Eur. Phys. J. Appl. Phys.* **2013**, *64* (3), 31302.

(33) Bormashenko, E.; Musin, A.; Zinigrad, M. Evaporation of Droplets on Strongly and Weakly Pinning Surfaces and Dynamics of the Triple Line. *Colloids Surf. A Physicochem. Eng. Asp.* **2011**, *385* (1), 235–240.

(34) Glycerine Producers' Association. *Physical Properties of Glycerine and Its Solutions*; Glycerine Producers' Association: New York, 1963.

(35) Joanny, J. F.; de Gennes, P. G. A Model for Contact Angle Hysteresis. *J. Chem. Phys.* **1984**, *81* (1), 552–562.

(36) Ozcelik, H. G.; Satiroglu, E.; Barisik, M. Size Dependent Influence of Contact Line Pinning on Wetting of Nano-Textured/Patterned Silica Surfaces. *Nanoscale* **2020**, *12* (41), 21376–21391.

(37) Orejon, D.; Shardt, O.; Gunda, N. S. K.; Ikuta, T.; Takahashi, K.; Takata, Y.; Mitra, S. K. Simultaneous Dropwise and Filmwise Condensation on Hydrophilic Microstructured Surfaces. *Int. J. Heat Mass Transf.* **2017**, *114*, 187–197.

(38) Yabumoto, N.; Minegishi, K.; Komine, Y.; Saito, K. Water-Adsorbed States on Silicon and Silicon Oxide Surfaces Analyzed by Using Heavy Water. *Jpn. J. Appl. Phys.* **1990**, *29* (3A), L490.

(39) Lohse, D.; Zhang, X. Surface Nanobubbles and Nanodroplets. *Rev. Mod. Phys.* **2015**, *87* (3), 981.

(40) Baudry, J.; Charlaix, E.; Tonck, A.; Mazuyer, D. Experimental Evidence for a Large Slip Effect at a Nonwetting Fluid－Solid Interface. *Langmuir* **2001**, *17* (17), 5232–5236.

(41) Teshima, H.; Takata, Y.; Takahashi, K. Adsorbed Gas Layers Limit the Mobility of Micropancakes. *Appl. Phys. Lett.* **2019**, *115* (7), 071603.